Electronic Supplementary Information (ESI)

Turn-on and blue-shift fluorescence sensor toward L-histidine based on stable Cd^{II} metal-organic framework with tetranuclear cluster units

Jing Li,[a] Shu-Li Yao,[a] Teng-Fei Zheng,[a]* Hui Xu,[a] Jin-Yan Li,[b] Yan Peng,[a] Jing-Lin Chen,[a] Sui-Jun Liu[a]* and He-Rui Wen[a]

[a]School of Chemistry and Chemical Engineering, Jiangxi University of Science and Technology, Ganzhou 341000, Jiangxi Province, P.R. China.

[b]School of Chemical and Environmental Engineering, Hanshan Normal University, Chaozhou 521041, Guangdong Province, P.R. China.

*Corresponding authors. E-mail: sjliu@jxust.edu.cn (S.-J. Liu), zhengtengfei0628@163.com (T.-F. Zheng). Tel: +86-797-8312204.

Table S1. Selected bond lengths (Å) and angles (°) for **JXUST-14**.[a]

Cd1—O1	2.4954(18)	Cd1—O2	2.2766(19)
Cd1—O4$^{\#1}$	2.2914(18)	Cd1—O4$^{\#2}$	2.4338(18)
Cd1—N7$^{\#3}$	2.389(2)	Cd1—O7$^{\#4}$	2.5287(19)
Cd1—O8$^{\#4}$	2.3209(19)	O1—Cd2$^{\#1}$	2.3097(19)
Cd2—O1$^{\#5}$	2.3097(19)	Cd2—O5	2.2645(19)
Cd2—O3	2.2664(18)	Cd2—O6	2.471(2)
Cd2—N6	2.356(2)	Cd2—O7$^{\#6}$	2.3302(18)
O4—Cd1$^{\#5}$	2.2914(18)	O4—Cd1$^{\#2}$	2.4338(17)
N7—Cd1$^{\#3}$	2.389(2)	O7—Cd1$^{\#7}$	2.5287(19)
O7—Cd2$^{\#6}$	2.3302(18)	O8—Cd1$^{\#7}$	2.3209(19)
O1—Cd1—O7$^{\#4}$	165.02(6)	O2—Cd1—O1	54.47(6)
O2—Cd1—O4$^{\#1}$	127.42(6)	O2—Cd1—O4$^{\#2}$	81.52(7)
O2—Cd1—N7$^{\#3}$	102.77(8)	O2—Cd1—O7$^{\#4}$	130.77(7)
O2—Cd1—O8$^{\#4}$	89.10(7)	O4$^{\#1}$—Cd1—O1	78.08(6)
O4$^{\#2}$—Cd1—O1	85.57(6)	O4$^{\#1}$—Cd1—O4$^{\#2}$	72.78(7)
O4$^{\#1}$—Cd1—N7$^{\#3}$	97.67(7)	O4$^{\#2}$—Cd1—O7$^{\#4}$	81.87(6)
O4$^{\#1}$—Cd1—O7$^{\#4}$	90.37(6)	O4$^{\#1}$—Cd1—O8$^{\#4}$	142.21(7)
N7$^{\#3}$—Cd1—O1	89.64(7)	N7$^{\#3}$—Cd1—O4$^{\#2}$	170.02(7)
N7$^{\#3}$—Cd1—O7$^{\#4}$	101.45(7)	O8$^{\#4}$—Cd1—O1	139.29(7)
O8$^{\#4}$—Cd1—O4$^{\#2}$	108.51(7)	O8$^{\#4}$—Cd1—N7$^{\#3}$	80.74(8)
O8$^{\#4}$—Cd1—O7$^{\#4}$	53.73(7)	Cd2$^{\#1}$—O1—Cd1	112.87(7)
O1$^{\#5}$—Cd2—O6	155.91(7)	O1$^{\#5}$—Cd2—N6	84.38(8)
O1$^{\#5}$—Cd2—O7$^{\#6}$	85.61(7)	O1$^{\#5}$—Cd2—C21	129.20(8)
O5—Cd2—O1$^{\#5}$	102.65(7)	O5—Cd2—O3	143.39(7)
O5—Cd2—O6	54.99(7)	O5—Cd2—N6	86.72(8)
O5—Cd2—O7$^{\#6}$	95.23(7)	O5—Cd2—C21	27.88(8)
O3—Cd2—O1$^{\#5}$	112.20(7)	O3—Cd2—O6	91.64(7)
O3—Cd2—N6	85.87(8)	O3—Cd2—O7$^{\#6}$	98.18(7)
N6—Cd2—O6	101.43(8)	O7$^{\#4}$—Cd2—O6	87.66(7)
O7$^{\#6}$—Cd2—N6	169.99(8)	Cd1$^{\#5}$—O4—Cd1$^{\#2}$	107.22(7)
Cd2$^{\#6}$—O7—Cd1$^{\#7}$	108.24(7)		

[a]Symmetry codes: #1: *x*, *y*, *z*-1; #2: -*x*+1, -*y*, -*z*; #3: -*x*+2, -*y*+1, -*z*; #4: *x*+1, *y*-1, *z*-2; #5: *x*, *y*, *z*+1; #6: -*x*, -*y*+1, -*z*+2; #7: *x*-1, *y*+1, *z*+2.

Table S2. SHAPE analysis of Cd^{II} ions in **JXUST-14**.

Ions	Label	Shape	Symmetry	Distortion(τ)
Cd1	HP-7	Heptagon	D_{7h}	29.730
	HPY-7	Hexagonal pyramid	C_{6v}	18.659
	PBPY-7	Pentagonal bipyramid	D_{5h}	4.213
	COC-7	Capped octahedron	C_{3v}	4.714
	CTPR-7	Capped trigonal prism	C_{2v}	**4.067**
	JPBPY-7	Johnson pentagonal bipyramid J13	D_{5h}	8.205
	JETPY-7	Johnson elongated triangular pyramid J7	C_{3v}	20.238
Cd2	HP-6	Hexagon	D_{6h}	32.417
	PPY-6	Pentagonal pyramid	C_{5v}	17.674
	OC-6	Octahedron	O_h	**4.538**
	TPR-6	Trigonal prism	D_{3h}	8.940
	JPPY-6	Johnson pentagonal pyramid J2	C_{5v}	21.930

Table S3. HOMO and LUMO energies for H_2BTDB and histidine.

	HOMO	LUMO
H_2BTDB	-0.220081 ev	-0.175782 ev
histidine	-0.180861 ev	-0.105947 ev

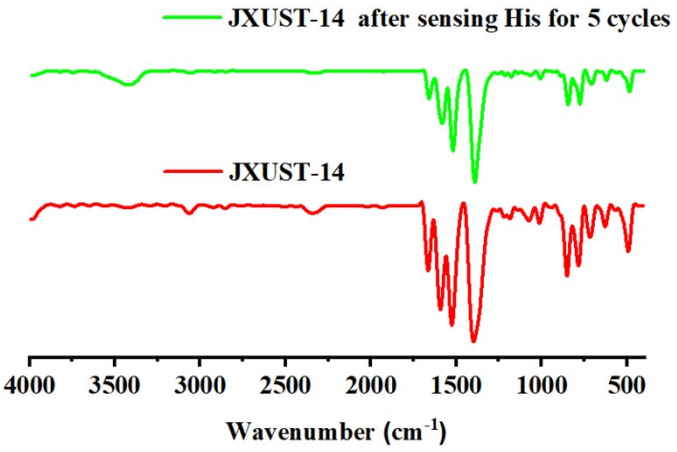

Fig. S1 IR spectra of **JXUST-14** and **JXUST-14** after sensing His for 5 cycles at room temperature.

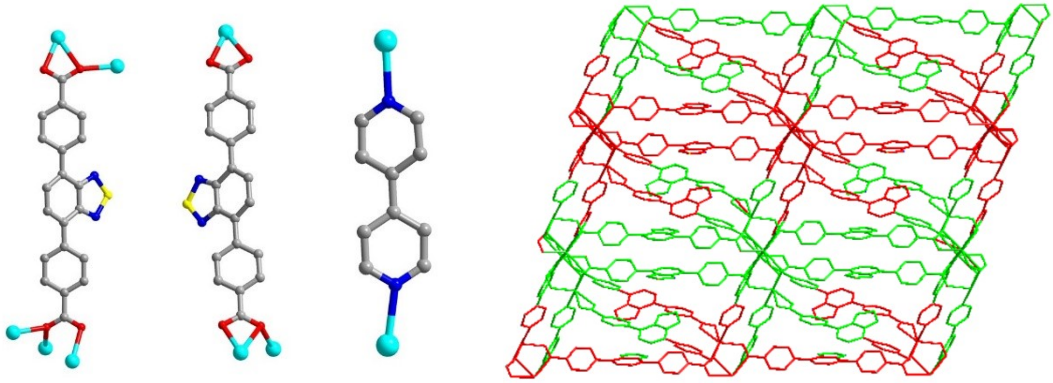

(a) **(b)**

Fig. S2 (a) View of the coordination modes of $BTDB^{2-}$ and 4,4-bpy in **JXUST-14**; (b) the two-fold interpenetrated structure of **JXUST-14**.

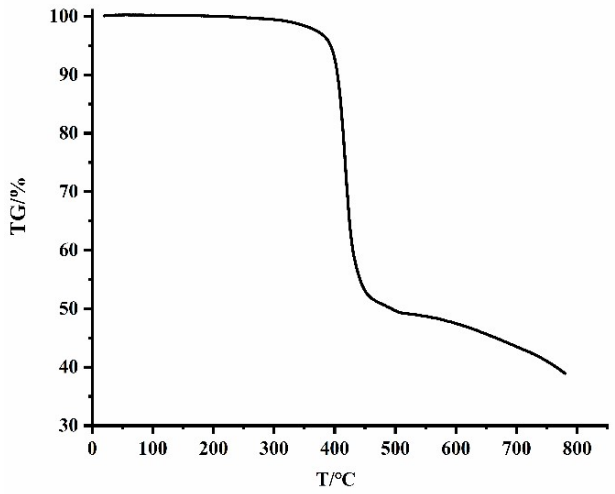

Fig. S3 The TGA curve for **JXUST-14** under N_2 atmosphere.

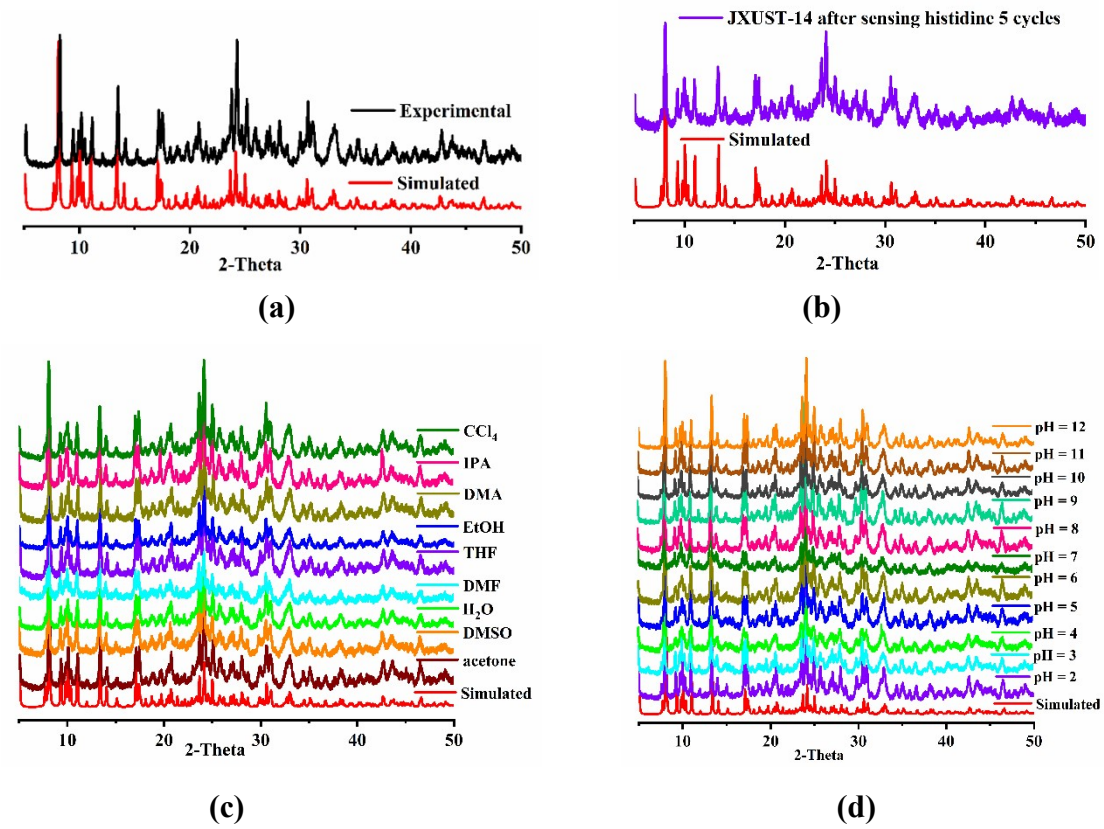

Fig. S4 (a) The simulated and experimental PXRD patterns of **JXUST-14**; (b) The simulated and experimental PXRD patterns of **JXUST-14** after sensing histidine for 5 cycles; (c) The simulated and experimental PXRD patterns of **JXUST-14** after immersing in common organic solvents for 48 h; (d) The simulated and experimental PXRD patterns of **JXUST-14** immersed in aqueous solution with diverse pH for 48 h.

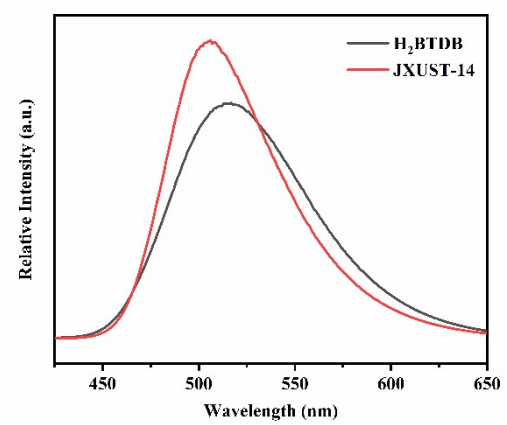

Fig. S5 Solid-state emission spectra of H_2BTDB and **JXUST-14**.

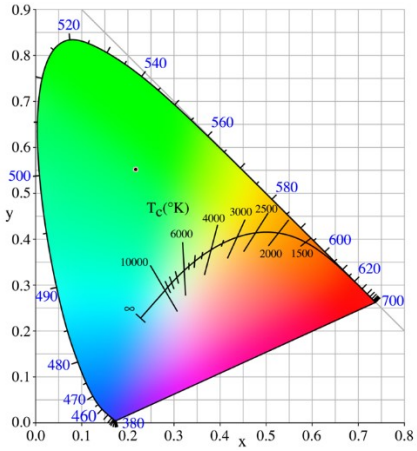

Fig. S6 CIE chromaticity diagram displaying the color coordinate of **JXUST-14**.

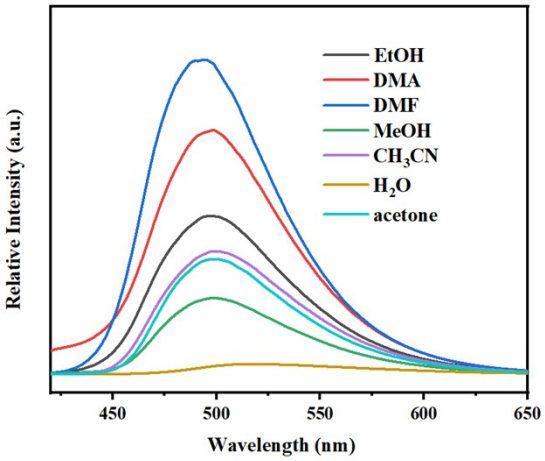

Fig. S7 The emission spectra of **JXUST-14** in some common solvents.

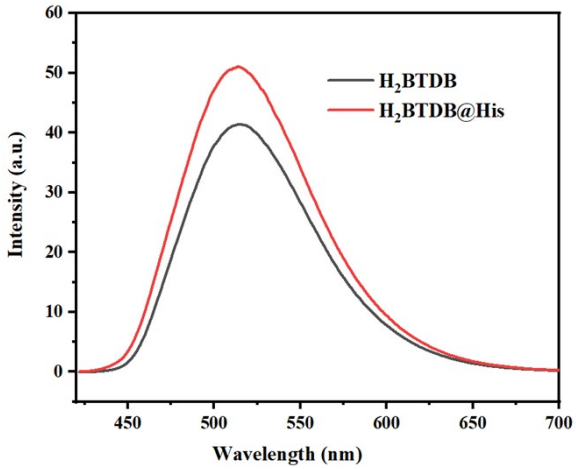

Fig. S8 The emission spectra of H_2BTDB ligand and H_2BTDB@His in EtOH solution.

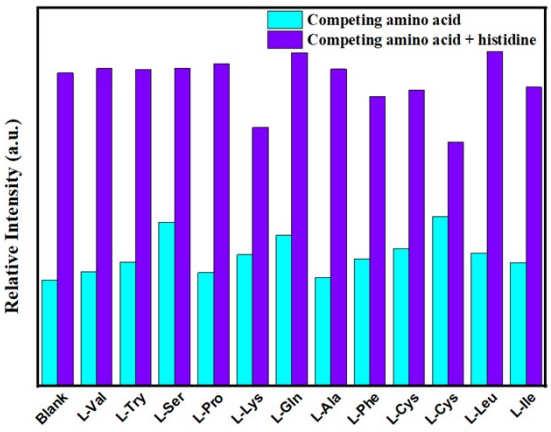

Fig. S9 Competitive experiments of **JXUST-14** in sensing histidine with the interference of other amino acids in EtOH solutions.

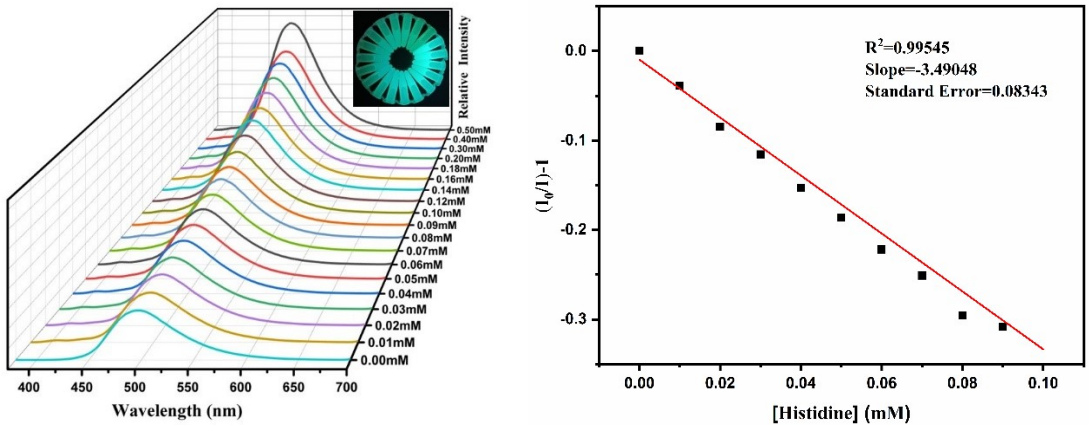

(a) **(b)**

Fig. S10 (a) Emission spectra of **JXUST-14** dispersed in EtOH suspension with various concentrations of histidine; (b) Linear relationship between fluorescence intensity and histidine concentration in a low concentration.

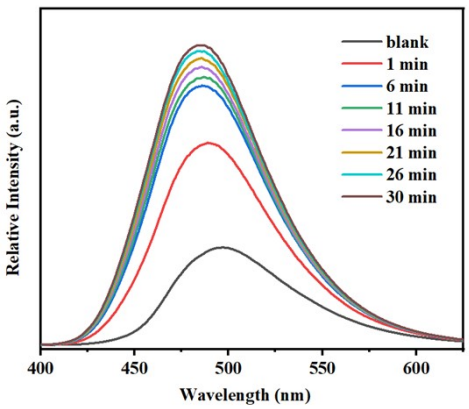

Fig. S11 Time-dependent emission spectra of **JXUST-14** after adding His.

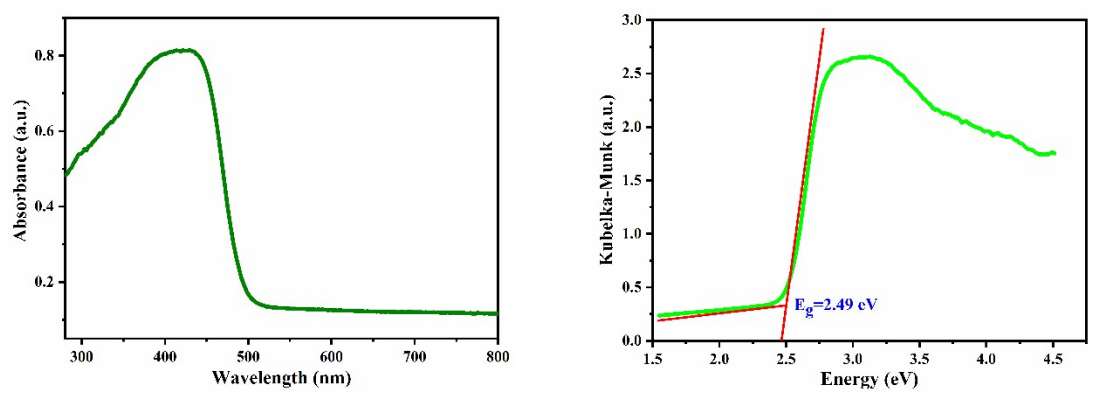

(a) **(b)**

Fig. S12 (a) UV-vis absorption spectra of **JXUST-14**; (b) the optical band gap diagram of **JXUST-14** calculated from the UV-vis absorption.

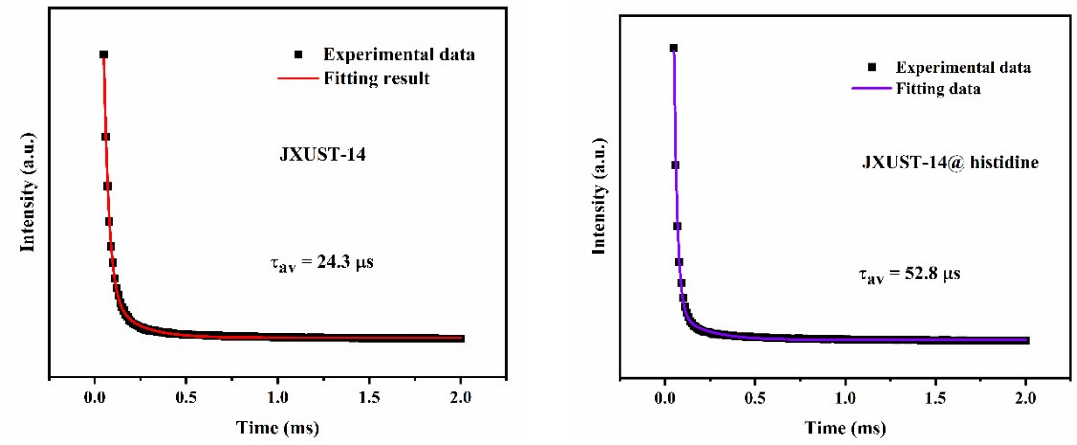

Fig. S13 The luminescence decay curves of **JXUST-14** and **JXUST-14@** histidine (1 mg **JXUST-14** dispersed in 2 mL DMF solution including 5 μL His with the concentration of 0.1 M).

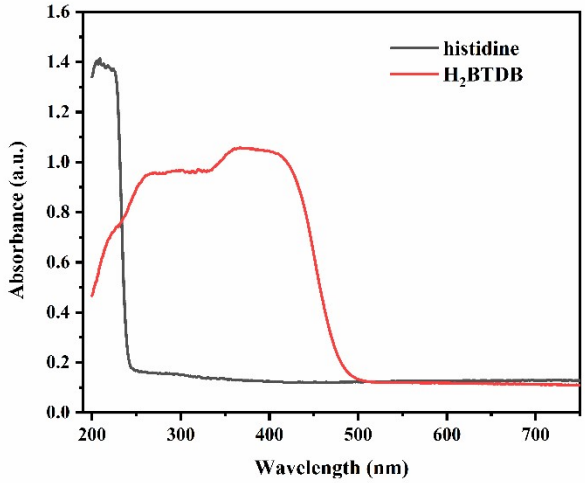

Fig. S14 The UV-vis absorption spectra of H_2BTDB ligand and histidine.